

Possibility of measurement of cosmic ray electron spectrum up to 100 TeV with two-layer water Cherenkov detector array

Andrii Neronov^{1,2}, and Dmitri Semikoz¹

¹*Université de Paris, CNRS, Astroparticule et Cosmologie, F-75006 Paris, France*

²*Astronomy Department, University of Geneva, Ch. d'Ecogia 16, 1290, Versoix, Switzerland*

Measurements of cosmic ray electron+positron spectrum above 10 TeV with ground-based experiments is challenging because of the difficulty of rejection of hadronic extensive air shower background. We study the efficiency of rejection of the hadronic background with water Cherenkov detector array supplemented by muon detection layer. We show that addition of a continuous muon detection layer to the experimental setup allows to achieve a $\sim 10^{-5}$ rejection factor for hadronic background at 10 TeV and enables measurement of electron spectrum in 10-100 TeV energy range. We show that measurements of electron spectrum in this energy range do not require a high-altitude experiment and can be done with a sea-level detector.

I. INTRODUCTION

Measurements of cosmic ray electron+positron spectrum using space and ground-based detectors are currently available up to 10 TeV energy range (see Ref. [1] for a review). The space-based detectors, like Fermi/LAT [2], AMS-02 [3], CALET [4], DAMPE [5], run out of signal statistics already at TeV energies. At higher energy, ground-based measurements have been done with HESS [6] and VERITAS [7] Imaging Atmospheric Cherenkov Telescope (IACT) systems up to approximately 5 TeV, and possibly to higher, ~ 20 TeV, energy by HESS [8].

These measurements reveal spectral features in the TeV band (Fig. 1), in part formed by an interplay between synchrotron and inverse Compton cooling of electrons in the interstellar magnetic and radiation fields [9, 10], but perhaps also by further effects of acceleration of primary electrons or production of secondary electrons and positrons in yet uncertain class of astronomical sources and their subsequent propagation through the Galaxy. The positron flux measured by AMS-02 is much lower than the overall electron plus positron flux level [3], thus the TeV softening of the spectrum visible in Fig. 1 certainly carries information about the nature of the electron source(s). The TeV suppression can be a feature introduced by the discreteness and intermittent nature of distribution of electron sources in the local Galaxy, like pulsars and supernova remnants [11] or can also be an average high-energy cutoff in the intrinsic spectra the source(s). It also can be an isolated feature superimposed on otherwise powerlaw-like spectrum. e.g. by a contribution from a specific nearby source [12].

To distinguish between these different possibilities, a better characterisation of the spectrum and reliable measurements of the flux extending well into the 10-100 TeV band are needed. Such an extension can hardly be done with space-based detectors, because the electron spectrum is very soft and relatively small area space-based detectors inevitably run out of statistics. The most promising possibility for extension of the measurements to higher energies is with the ground-based detectors. Ground-based experiments detect electrons and

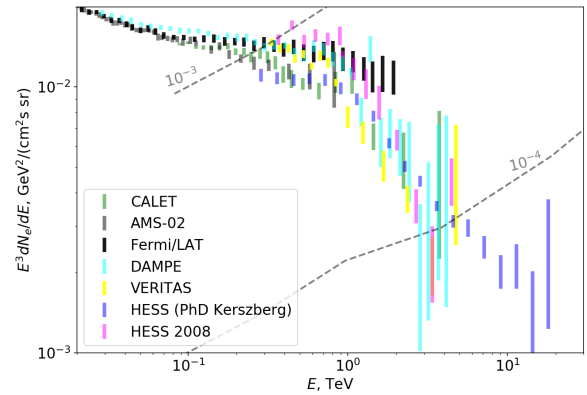


FIG. 1: Measurements of e^+e^- spectrum by AMS-02 [3], Fermi/LAT [2], DAMPE [5], CALET [4], HESS [6], [8], VERITAS [7]. Dashed lines show different levels of rejection of background of cosmic ray nuclei needed to detection of flux as a given level.

positrons by observing Extensive Air Showers (EAS) that they initiate while penetrating into the atmosphere. The main challenge of the ground-based measurement is to distinguish the signal of electron induced EAS from the background of EAS initiated cosmic ray protons and atomic nuclei. The electron flux is at the level of $\lesssim 10^{-4}$ of the nuclei flux at 10 TeV, see Fig. 1. Different dedicated background rejection techniques based on fitting of numerically predicted templates of "electron-like" EAS images to the observed EAS image data have been used to achieve rejection of proton and nuclei background in the HESS data [6, 8, 13–15]. The difficulty of this approach can be illustrated by comparison of the HESS measurement up to 20 TeV reported in conference proceedings [8] and several PhD theses [13–15], with different types of background rejection techniques providing different results and indicate a large systematic uncertainty of the analysis.

An alternative possibility for discrimination between the EAS induced by protons and atomic nuclei and EAS

induced by electrons and positrons is provided by the measurement of muon content of the EAS. This technique is used by KASCADE [16], Carpet-2 [17] and LHAASO [18] experiments to measure the identity of the primary cosmic ray particles in the energy range above 100 TeV or above 1 PeV. Extension of the "muon tagging" approach for cosmic ray proton and nuclei background suppression toward lower energies is considered for the SWGO experiment [19]. It is however challenging because of decrease of density of muons on the ground associated to the decrease of the energy of the primary cosmic ray particles.

Below we show that a deployment of a large continuous muon detector counting (rather than just sampling) muons at the detection level is necessary to achieve efficiency of rejection of hadronic EAS background by a factor $> 10^5$ needed for the measurement of e^+e^- spectrum in 10-100 TeV energy range. We discuss possible implementations of such large muon detector.

II. LARGE WATER CHERENKOV MUON DETECTOR FOR 10-100 TEV EAS

Muons are conventionally detected in the EAS experiments by particle detectors, like scintillator pads (e.g. in Carpet-2 experiment [17]) or water tanks (like in LHAASO experiment [18]) buried underground, or shielded by dense material layer (like in KASCADE experiment [16]). Otherwise, muons can also be identified in surface Water Cherenkov Detector Arrays (WCDA) like those of HAWC [20] and LHAASO because they produce much larger Cherenkov light signal with specific timing signature, due to the deep penetration. Muon identification in WCDA placed on the surface (rather than under-ground) is difficult because of the mixing of the muon Cherenkov light signal with the signal of electromagnetic EAS component. Finally, deep underwater Cherenkov detectors, like ANTARES [21], Baikal-GVD [22] and Km3NET [23] are able to track trajectories of individual muons and measure their energy, to obtain information about neutrinos that produce muons in interactions with material surrounding the detector.

10-100 TeV EAS produced by protons generate only $10^2 - 10^4$ muons scattered across large area within ~ 400 m around the shower axis [24, 25], so that the muon density is as low as $\leq 10^{-2}$ m². Low density of muons on the ground complicates their detection. A muon passing through water with the speed faster than the speed of light in the medium generates some $Y_{Ch} \simeq 200$ ph/cm Cherenkov photons in the 400-700 nm wavelength range. The number of photoelectrons detectable by a large (e.g. $d_{pmt} = 10'' = 25$ cm) photomultiplier tube (PMT) with photon detection efficiency κ placed at a distance R from the particle track is $n_{p.e.} \simeq Y_{Ch} d_{pmt}^2 / (8R \tan(\theta_{Ch})) \simeq 5 [\kappa/0.3] [d_{pmt}/25 \text{ cm}]^2 [R/10 \text{ m}]^{-1}$ where $\theta_{Ch} \simeq 41^\circ$ is the Cherenkov angle in water. Adopting $n_{p.e.} \sim 5$ as a threshold for detection of particle track in water Cherenkov detector, we find that single large photo-

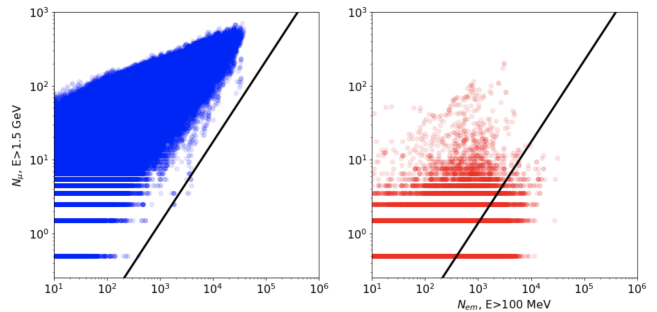


FIG. 2: Muon+hadron vs Electron-positron-gamma counts for the EAS impacting the 150×150 m² area of μ WCDA for proton induced EAS (left) and electrons (right). We have replaced zero muon counts with "0.5 count" value, to show the EAS without muon counts in this logarithmic plot. Black line shows possible electron-hadron separation cut.

multiplier tube can detect muons passing at a distance as large as $R \simeq 10 [d_{pmt}/25 \text{ cm}]^2$ m. Thus, deployment of optical sensors on a sparse grid with spacing smaller $\sim 2R$, in a light-tight compartment at a depth range between 5 m and 5 m+ R (to suppress the electron/positron/gamma component of the EAS) can be sufficient.

The 10-100 TeV EAS are able to reach the sea level and it is in principle not necessary to place the large muon detector at high altitude. This allows to directly use the optical modules of neutrino telescopes like ANTARES [26] or Baikal-GVD [27] and deploy the detector in the same water reservoir as the original neutrino detector (sea or lake), partially re-using the available experimental infrastructure. Otherwise, the WCDA consisting of two-layer water tanks like foreseen for SWGO [19] can be considered.

To determine the efficiency of the muon detector necessary for "muon tagging" of proton and nuclei induced EAS we have performed Monte-Carlo simulations of EAS using CORSIKA package (<https://www.iap.kit.edu/corsika/index.php>, version 75600). We have assumed two-layer detector setup at sea level altitude with the top layer counting particles with energies at least 100 MeV crossing the water surface and bottom layer sampling muons and hadrons with energies at least 1.5 GeV reaching the 5 m depth.

The electron flux is by up to five orders lower than the overall cosmic ray flux in the 10-100 TeV energy range (see Fig. 1). Thus, the detector has to assure that no more than 1 in 10^5 hadronic EAS is mis-interpreted as an electron / positron induced EAS. To verify this, we have simulated 7×10^5 proton-induced EAS in the broad energy range 1-100 TeV and 10^4 electron-induced EAS, saving the particle content on the ground (hadrons and muons with energies above 300 MeV, electrons, positrons and gammas with energies above 30 MeV). The EAS were allowed to impact anywhere within the extent of the detector.

The statistics of electrons, positrons and gammas with energies above 100 MeV, N_{em} and statistics of muon and hadron counts with $E > 1.5$ GeV for all EAS is shown in Fig. 2 for the selection of EAS falling within 150×150 m² central part of a 300×300 m² detector, 100% efficient in counting both electromagnetic cascade particles and muons. To reject the hadronic EAS background, we have considered a cut shown by the straight line in Fig. 2 (cut optimisation has to be a subject of dedicated study). Only events to the right of the cut line or events with $N_{\mu} = 0$ were accepted.

If the muon layer of the detector is not continuous, only a fraction of the muons reaching the ground level would be counted. For example, LHAASO muon detector component covers only about 4% of the area. This reduces the statistics of the muon signal and hence the efficiency of electron-hadron shower discrimination. We have verified that our method of estimation of hadronic background rejection is consistent with the published estimated of background rejection efficiency for LHAASO [18] if we assume that only 4% of the muons are detectable. This is illustrated in Fig. 3, where we compare the efficiency of rejection of proton shower background for different efficiencies of muon detection: 0.04 (LHAASO-type muon detector), 0.2 and 1 (continuous muon detector like that foreseen fro SWGO). One can see that deployment of continuous detector is necessary if one aims at background rejection level $\sim 10^{-5}$ at 10 TeV. Deployment of muon detectors on a grid two times denser than that implemented in LHAASO would still not be sufficient. This result does not depend on the assumption about the altitude of the detector. In our simulations we counted muons reaching the sea level, but the number of muons does not change significantly with altitude in a wide altitude range, from 0 to about 4.5 km for the energy range of interest. We have verified this by repeating the simulations for the detector at 4.5 km altitude.

The altitude of the detector most strongly affects the statistics of the electromagnetic shower component. Decrease of the number of electromagnetic cascade particles at low altitude increases the energy threshold of the experiment. This is illustrated in Fig. 4 in which the thick blue dashed line shows the energy dependence of efficiency of selection of electron EAS for the sea-level detector. This efficiency approaches ~ 0.5 in the energy range above 10 TeV. The decrease of efficiency below 10 TeV is explained by the "quality" cut $N_{em} > 100$ that we have imposed on the selection of both proton and electron events. We have imposed this cut to assure that the detected events can be properly analyzed and their energy estimated with reasonable accuracy). Also this cut has to be optimized via a detailed study for specific detector setups. The same cut for a detector at 4.5 km altitude provides a nearly 100% detection efficiency for electron showers down to TeV energy (thin dashed line).

The HAWC and LHAASO WCDA have areas com-

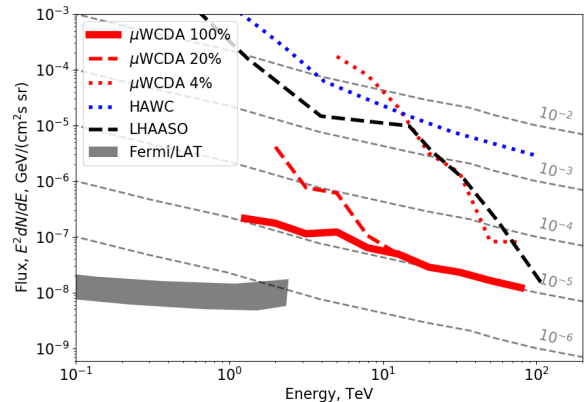


FIG. 3: Residual cosmic ray proton and nuclei background level for the setup with the muon detector layer underlying 100% (red thick solid line), 20% (dashed thin red line) and 5% (red dotted line) of WCDA. For comparison we show the background levels in selected detectors: LHAASO (black thin solid line) and HAWC (blue thin solid line).

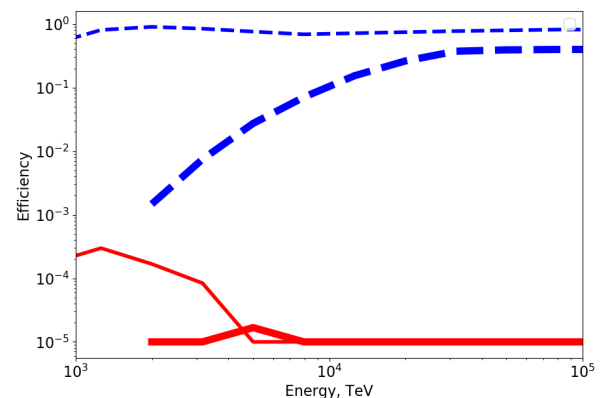


FIG. 4: Efficiency of the cut separating hadronic and e^+e^- EAS as a function of energy, for electrons (blue dashed lines) and protons (red solid lines) for a detector at sea level (thick lines) and at 4.5 km altitude (thin lines).

parable to or larger than that of the muon continuous detector considered in our analysis. In principle, both WCDA can detect all muons passing through them. They can also distinguish muon signal from the signal of electromagnetic EAS component, because single muons crossing the full depth of the water tanks produce larger Cherenkov signal. However, from Fig. 3 one can see that in spite of detecting similar amount of muons in 10-100 TeV EAS, HAWC and LHAASO WCDA do not reach the efficiency of rejection of hadronic EAS comparable to that of the large muon detector. This is explained by the difficulty of identification of the muon signal on top of strong electromagnetic signal that dominates the EAS signal in WCDA not screened by the 5 m

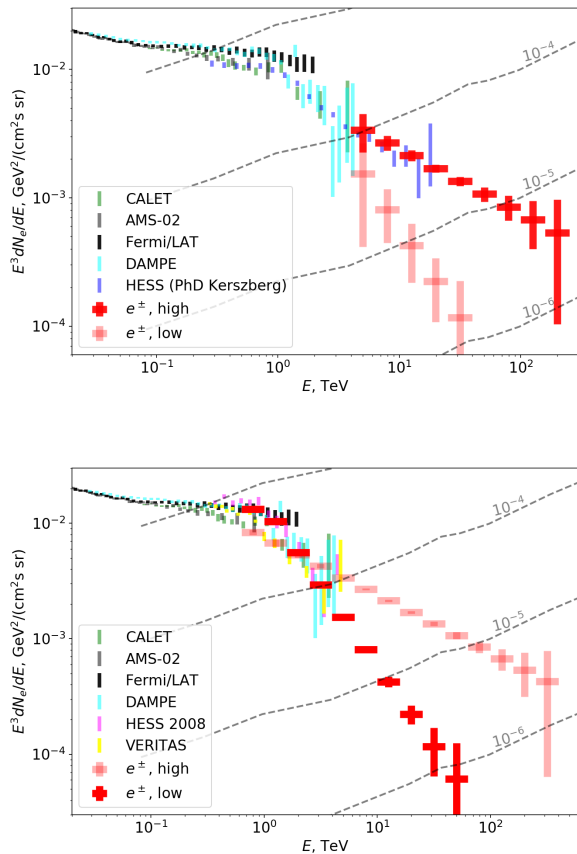


FIG. 5: Expected quality of electron spectrum measurement with WCDA detector with 100% efficient muon detection layer at sea level altitude (top), and at 4.5 km altitude (bottom). Experimental data are the same as in Fig. 1. Two possible high-energy powerlaw extrapolations are considered, with higher and lower flux levels with opaque and semi-transparent red color. Full red color highlights the high flux (top) and low flux (bottom) extrapolations for respectively the sea level and high-altitude detectors.

water depth. Thus, an efficient μ WCDA has to include a dedicated muon detection layer, rather than aim at muon detection on top of a dominant electromagnetic signal in single WCDA layer.

Efficient suppression of hadronic background in WCDA with continuous muon detection layer enables measurement of electron spectrum in the energy range above 10 TeV. This is shown in Fig. 5. The top panel of this figure shows numerically estimated quality of measurements of electron spectrum with the sea-level detector for possible "high" and "low" flux extrapolations of the electron spectrum measurements into 10-100 TeV range. To make these estimates we have assumed that the effective collection area for both proton background and electrons is the geometrical area of the detector times the efficiency of electron selection shown in Fig. 4. The angular acceptance of the WCDA is assumed to be 30°

around zenith, the exposure time is one year. The errorbars are determined by the statistical error for the electron signal detected on top of the residual hadronic background. A systematic error at the level of 5% of the hadronic background is added.

One can see that the flux at the level of the high flux powerlaw extrapolation from sub-10-TeV range is readily detectable up to 100 TeV and beyond on top of the residual hadronic background with an experimental setup using the 100% efficient muon detection layer. Remarkably, the electron spectrum can, in principle, be measured starting from the TeV energy range, in spite of the low efficiency of electron detection with an experimental setup at the sea level altitude. This is explained by the steepness of electron spectrum. The electron flux becomes as high as $\sim 10^{-3}$ of the cosmic ray flux at TeV. Even if the efficiency of electron detection is as low as 10^{-3} at this energy, suppression of the background of cosmic ray nuclei by a factor $\sim 10^{-5}$ still leaves the electron signal statistics at the level of about 10% of the nuclei background statistics.

If the electron spectrum above 1 TeV is as steep as the lowest flux allowed by VERITAS [7] or the 2008 HESS [6] measurements (this would mean that the most recent HESS analysis [8, 13] still suffers from residual hadronic background contamination), the electron count statistics in a sea-level detector decreases below the residual cosmic ray nuclei statistics in all energy bins. This explains large errorbars of the measurements for this case (lower pale red data points in the top panel of Fig. 5). In this case it might be essential to increase the efficiency of detection of electromagnetic component of the EAS, either by supplementing the sea-level detector with an IACT system or by deploying the detector at high altitude, as foreseen in the SWGO design. The expected improvement of the quality of measurements with the high-altitude detector is shown in the bottom panel of Fig. 1 where the expected quality of measurements of electron spectrum with a two-layer WCDA at 4.5 km altitude is shown. The high-altitude and sea-level detectors provide similar quality of measurements above approximately 20 TeV. At lower energies, only the high altitude setup has sufficiently high efficiency of detection of electron induced EAS to provide high quality measurement. One can see that in this case, the electron spectrum measurements can also have a good overlap with the measurements by space-based detectors.

III. DISCUSSION AND CONCLUSIONS

We have shown that measurements of cosmic ray e^+e^- spectrum up to 100 TeV are possible using an experimental setup that includes an EAS array that provides nearly 100% efficiency of muon detection across a $150 \times 150 \text{ m}^2$ area. Such a detector can be implemented as an underwater Cherenkov detector combined with a conventional WCDA, as foreseen in the design of SWGO. Moreover, if

the electron flux level at 10 TeV is as high as suggested by the most recent HESS data analysis, such detector does not necessarily need to be located at high altitude.

The most straightforward possibility for the sea-level setup is to implement the under-water muon detector re-using the development of water-Cherenkov neutrino detectors. The optical modules of neutrino detectors like ANTARES [21], Baikal-GVD [22] or Km3NET [23] can be directly deployed at shallow depth in a two-storey grid (at depths about 5 and 10-15 m) within light-tight sec-

tions. Estimates of the Cherenkov light intensity show that the layout of the muon detection layer can be rather sparse, with module separation up to 20 m if large 12" photo-multiplier tubes are used. In the absence of the high-altitude constraint, the large shallow depth water-Cherenkov detector array can even be implemented directly at the sites of the underwater neutrino observatories, to simultaneously serve as a part of cosmic ray veto for the neutrino experiment (similar to the IceTop array at the site of IceCube experiment).

-
- [1] P. Lipari (2019), 1902.06173.
- [2] S. Abdollahi et al. (Fermi-LAT), *Phys. Rev. D* **95**, 082007 (2017), 1704.07195.
- [3] M. Aguilar et al. (AMS), *Phys. Rev. Lett.* **122**, 101101 (2019).
- [4] O. Adriani et al. (CALET), *Phys. Rev. Lett.* **119**, 181101 (2017), 1712.01711.
- [5] G. Ambrosi et al. (DAMPE), *Nature* **552**, 63 (2017), 1711.10981.
- [6] F. Aharonian et al. (H.E.S.S.), *Phys. Rev. Lett.* **101**, 261104 (2008), 0811.3894.
- [7] A. Archer et al. (VERITAS), *Phys. Rev. D* **98**, 062004 (2018), 1808.10028.
- [8] D. Kerszberg et al. (HESS), International Cosmic Ray Conference (2015), URL <https://indico.snu.ac.kr/indico/event/15/session/5/contribution/694/material/slides/0.pdf>.
- [9] F. A. Agaronian and A. S. Ambartsumian, *Astrofizika* **23**, 479 (1985).
- [10] L. Stawarz, V. Petrosian, and R. D. Blandford, *Astrophys. J.* **710**, 236 (2010), 0908.1094.
- [11] A. M. Atoyan, F. A. Aharonian, and H. J. Völk, *Phys. Rev. D* **52**, 3265 (1995).
- [12] S. Recchia, S. Gabici, F. A. Aharonian, and J. Vink, *Phys. Rev. D* **99**, 103022 (2019), 1811.07551.
- [13] D. Kerszberg, PhD Thesis, University Pierre et Marie Curie (2017), URL <https://tel.archives-ouvertes.fr/tel-01682782/document>.
- [14] M. Kraus, PhD Thesis, University of Erlangen (2018), URL https://ecap.nat.fau.de/wp-content/uploads/2018/07/2018_Kraus_Dissertation.pdf.
- [15] D. Koltzhus, PhD Thesis, University of Innsbruck (2016), URL <https://diglib.uibk.ac.at/ulbtirolns/download/pdf/1188076?originalFilename=true>.
- [16] W. Apel et al. (KASCADE Grande), *Astrophys. J.* **848**, 1 (2017), 1710.02889.
- [17] D. Dzhappuev et al., *JETP Lett.* **109**, 226 (2019), 1812.02662.
- [18] X. Bai et al. (2019), 1905.02773.
- [19] A. Albert et al. (2019), 1902.08429.
- [20] A. Zuñiga Reyes, A. Hernández, A. Miranda-Aguilar, A. Sandoval, J. Martínez-Castro, R. Alfaro, E. Belmont, H. León, and A. P. Vizcaya (HAWC), *PoS ICRC2017*, 750 (2018), 1708.09500.
- [21] E. Aslanides et al. (ANTARES) (1999), *astro-ph/9907432*.
- [22] A. Avrorin et al. (Baikal-GVD), *PoS ICRC2019*, 1011 (2020), 1908.05427.
- [23] P. Bagley et al. (KM3NeT) (2009).
- [24] T. Antoni et al. (KASCADE), *Astropart. Phys.* **14**, 245 (2001), *astro-ph/0004233*.
- [25] A. Lagutin and R. Raikin, *Nuclear Physics B - Proceedings Supplements* **97**, 274 (2001), ISSN 0920-5632, URL <http://www.sciencedirect.com/science/article/pii/S0920563201012828>.
- [26] P. Amram et al. (ANTARES), *Nucl. Instrum. Meth. A* **484**, 369 (2002), *astro-ph/0112172*.
- [27] A. Avrorin et al., *EPJ Web Conf.* **116**, 01003 (2016).